CHAPTER IV
RESULTS AND DISCUSSION

The kinetics of oxide formation for each materials; carbon steel (CS A106B), stainless steel (SS 316) and nickel alloy (Alloy 625) was investigated. Due to the low rate of oxide formation on SS 316 and Alloy 625, therefore, this study was mainly focused on the kinetics of oxide formation on CS A106B. However, the surface analyses of all materials are discussed in this chapter.

The kinetics of oxide formation of CS A106B was separated into two parts; oxide formation on the surfaces which were exposed to an atmosphere with no change in O_2 concentration, and oxide formation on the surfaces which were exposed to an atmosphere with change in O_2 concentration.

The study of oxide formation on the surfaces which were exposed to an atmosphere with changing O_2 concentrations also includes the study of the pressure change in the cavity. This pressure change was related to the rate of oxide formation which was determined by the weight change on the carbon steel sample. Results and discussion are provided as follows.

4.1 Materials Characterization

4.1.1 Baseline Analysis

The sample of each material was analyzed before the experiment to obtain baseline data for each material.

SEM images show fresh polished surfaces which were polished and stored in a desiccator for 14 days. The images (Figure 4.1) show surfaces without oxide particles. Some scratches which might occur from the polishing steps were observed.

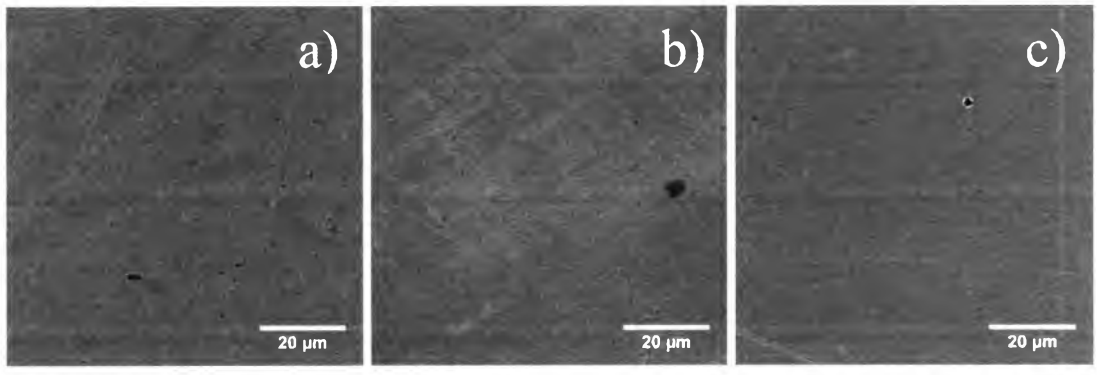

Figure 4.1 SEM image of baseline surfaces; a) carbon steel, b) stainless steel and c) nickel-alloy.

Each material was also examined by EDS which gives the elemental composition on the metal surfaces. The CS A106B is a low chrome carbon steel which has chromium less than 0.5wt%.

The extra surface which was required to reach the area-to-volume ratio of the practical construction unit was chosen from a wire which has a similar elemental composition. The extra surface of carbon steel and stainless steel were chosen from materials which have similar wt% content of Fe and Cr to the membrane. In case of nickel-alloy, extra surface material was selected from an available Ni/Cr wire which has closest Ni and Cr content to the alloy 625.

The elemental analyses are shown in Table 4.1 for the membranes and Table 4.2 for the extra surfaces.

Table 4.1 Elemental analysis results of baseline samples (membranes)

Samples	Element (Wt %)							
	O	**Si**	**Nb**	**Mo**	**Cr**	**Fe**	**Ni**	**Total**
CS A106B								
Spectrum 1	1.97	0.38	0.06	0.10	0.07	97.43	0.00	100
Spectrum 2	2.06	0.41	0.00	0.66	0.11	96.76	0.00	100
Spectrum 3	2.14	0.40	0.19	0.07	0.16	97.05	0.00	100
Average	2.06	0.40	0.08	0.28	0.11	97.08	0.00	100
SS 316								
Spectrum 1	3.46	0.56	0.22	1.99	17.06	67.66	9.05	100
Spectrum 2	3.37	0.58	0.00	2.05	17.29	67.14	9.58	100
Spectrum 3	3.45	0.63	0.08	2.15	17.26	66.68	9.74	100
Average	3.43	0.59	0.10	2.06	17.20	67.16	9.46	100
Alloy 625								
Spectrum 1	4.27	0.42	3.51	8.05	21.73	3.51	58.51	100
Spectrum 2	3.61	0.20	3.83	8.82	21.85	3.59	58.10	100
Spectrum 3	3.53	0.22	3.79	8.89	22.12	3.56	57.89	100
Average	3.80	0.28	3.71	8.59	21.90	3.55	58.17	100

Table 4.2 Elemental analysis results of extra surface samples (wires)

Samples	Element (Wt %)										
	O	**Al**	**Si**	**P**	**Mo**	**Ca**	**Cr**	**Fe**	**Ni**	**Zn**	**Total**
CS-wire											
Spc. 1	2.11	0.13	0.25	0.03	0.29	0.10	0.41	95.82	0.4	0.46	100
Spc. 2	2.55	0.24	0.27	0.09	0.20	0.16	0.14	96.35	0.0	0.00	100
Average	2.33	0.19	0.26	0.06	0.25	0.13	0.28	96.09	0.2	0.23	100
SS-wire											
Spc. 1	3.92	0.08	0.56	0.09	0.33	0.15	18.73	66.94	8.6	0.61	100
Spc. 2	5.19	0.20	0.62	0.03	0.20	0.08	18.73	66.10	8.5	0.38	100
Average	4.56	0.14	0.59	0.06	0.27	0.12	18.73	66.52	8.5	0.50	100
NI-wire											
Spc. 1	4.42	0.35	1.58	0.12	0.31	0.19	20.82	0.47	71.6	0.15	100
Spc. 2	4.34	0.36	1.50	0.06	0.21	0.17	20.77	0.44	72.1	0.00	100
Average	4.38	0.36	1.54	0.09	0.26	0.18	20.80	0.46	71.9	0.08	100

4.1.2 Carbon Steel (CS A106B)

SEM images show the carbon steel surfaces after the 400°C exposure (Figure 4.2). On the B side (which was exposed to the environment without change in oxygen concentration during the exposure), the form of oxide films is micaceous, but with different size due to the exposure time. The longer the exposure time, the bigger the sizes of the flakes. The Raman spectra (Figure 4.3) show that these oxides are Hematite (Fe_2O_3).

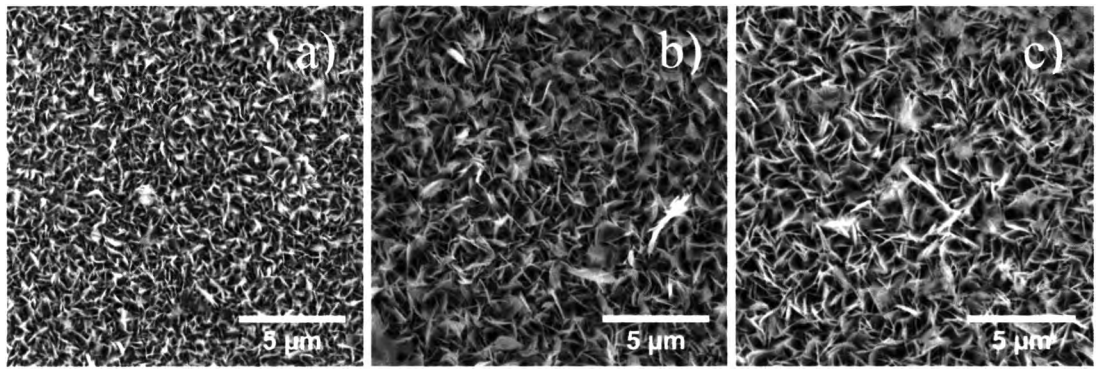

Figure 4.2 SEM images of B-side carbon steels exposed to the free air; a) 1 day, b) 7 days and c) 14 days.

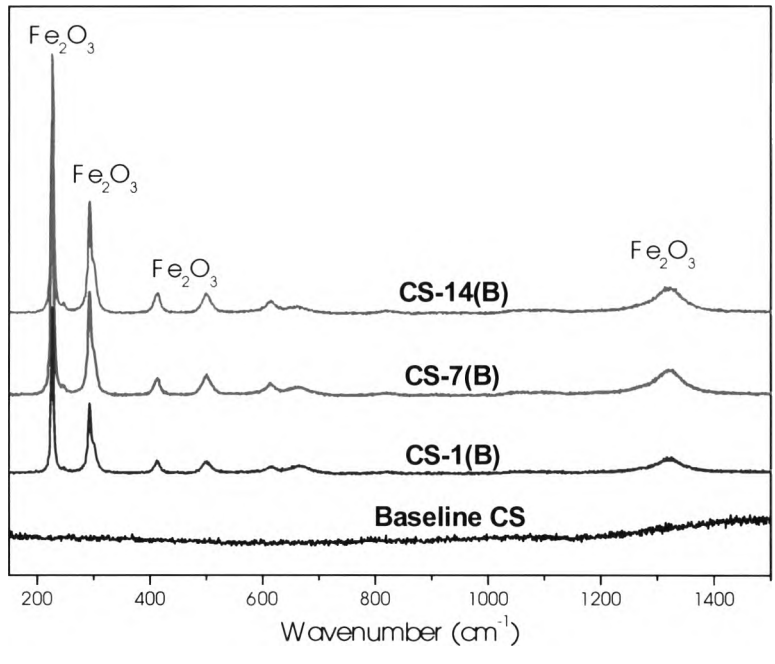

Figure 4.3 Raman spectra of B-side carbon steels exposed to the free air for 1 day (CS-1(B)), 7 days (CS-7(B)) and 14 days (CS-14(B)).

In the first set of experiments, the forms of oxide on A side (which was exposed to the environment with change in oxygen concentration during the exposure) are different; for the 1 and 7 day exposure, the form of oxide is mainly micaceous (Figures 4.4 (a) and 4.4 (b)). Also Raman spectra (Figure 4.5) show that

these oxides are mainly Hematite (Fe_2O_3). The oxide form of 14 day exposure (Figure 4.6 c) is granular Magnetite (Fe_3O_4).

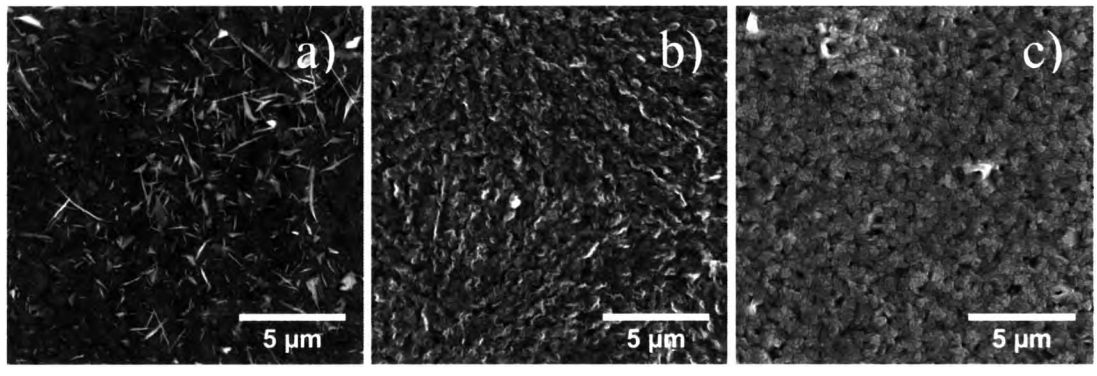

Figure 4.4 SEM images of A-side carbon steels in the first set of experiments exposed to the simulated environment; a) 1 day, b) 7 days and c) 14 days.

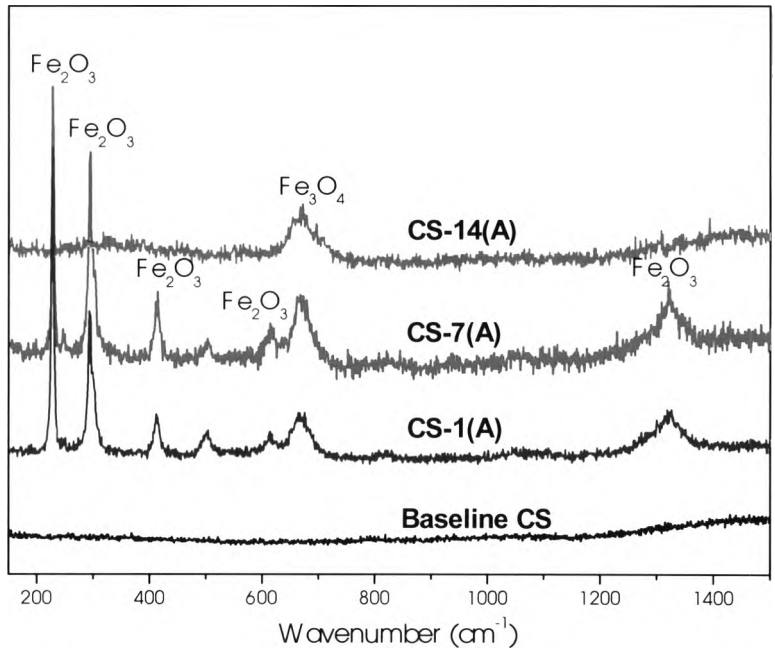

Figure 4.5 Raman spectra of A-side carbon steels in the first set of experiment exposed to the simulated environment for 1 day (CS-1(A)), 7 days (CS-7(A)) and 14 days (CS-14(A)).

The second set of experiments was performed in order to confirm the oxide type formed on the surfaces which were exposed to an atmosphere with change in O_2 concentration (A-side). Figure 4.6 show images of oxide film on each sample. Magnetite was found on 7 days and 1 day exposures, however, on 5 hours exposure some Hematite was found. From Raman spectra, the mixture of Magnetite and Hematite was found on some parts of surface (Figure 4.7: CS-5hr(A2)-2) and the characteristic peak of Hematite was a weak peak, which means the area is mainly Magnetite.

Type and shape of oxide formed at 400°C depend on the oxygen concentration in an environment of the exposure. Magnetite formed if the environment has lower oxygen concentration. The difference of oxygen concentration is discussed in 4.3.4.

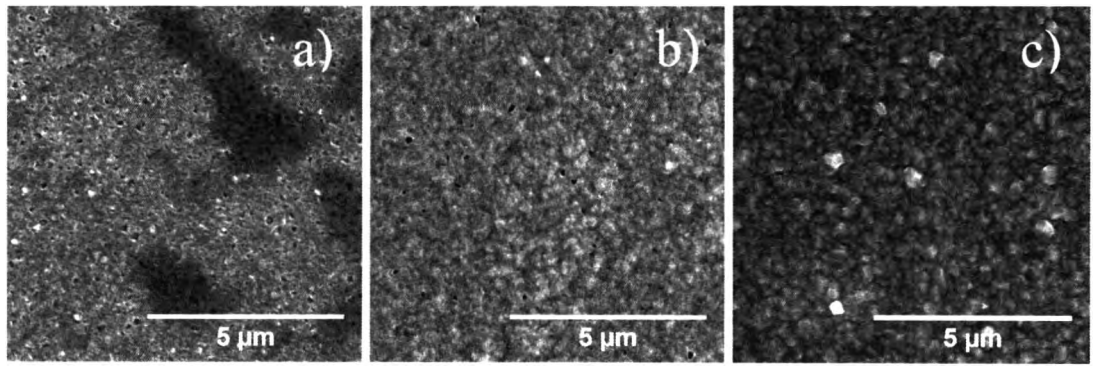

Figure 4.6 SEM images of A-side carbon steels in the second set of experiments exposed to the simulated environment; a) 5 hours, b) 1 day and c) 7 days.

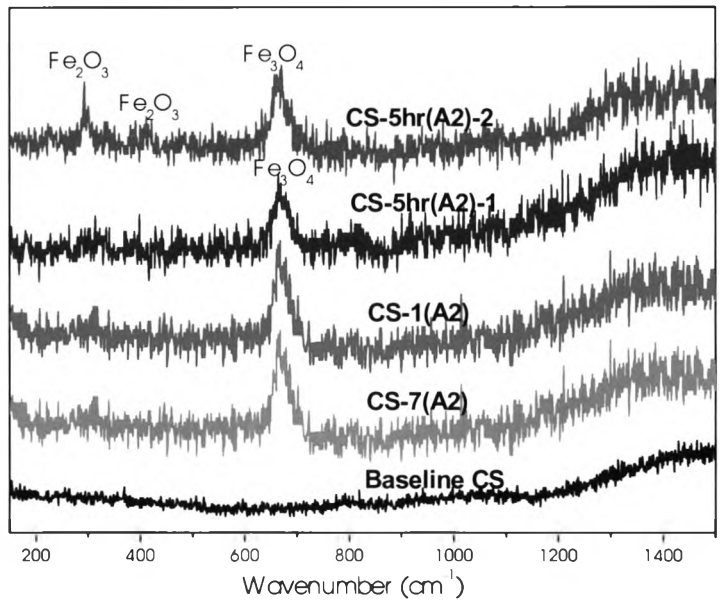

Figure 4.7 Raman spectra of A-side carbon steels in the second set of experiments exposed to the simulated environment for 5 hours (CS-5hr(A2)), 1 day (CS-1(A2)) and 7 days (CS-7(A2)).

For the membrane exposed to 90°C for 14 days, color change and oxide formation were not observed. The surface images and the Raman spectra of the membrane were the same as the fresh polished membrane. SEM images show the carbon steel surface from 90°C exposure; there are no differences between the surfaces of A-side and B-side and they are the same as fresh polished surfaces.

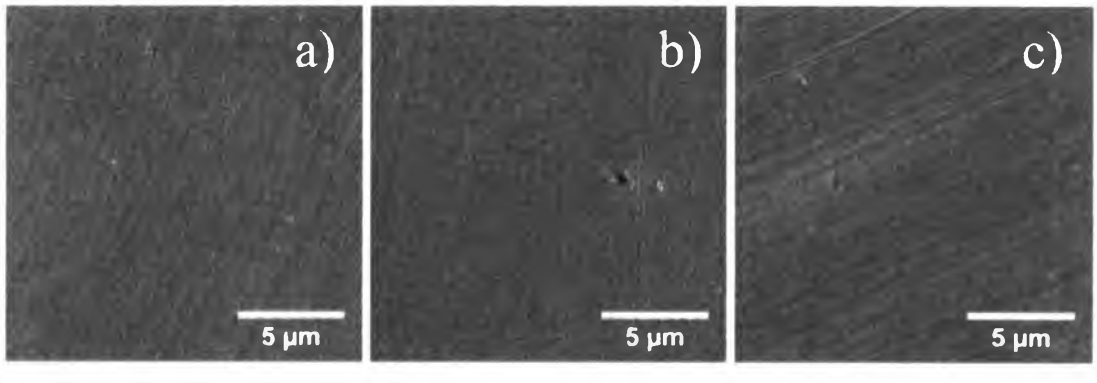

Figure 4.8 SEM images of carbon steel surfaces exposed to 90°C for; a) 1 day, b) 7 days and c) 14 days.

4.1.2.1 Thermodynamic Equilibrium

Equilibrium using thermodynamic data was determined to predict the oxide type that will form on the carbon steel surfaces at each environment. The results from the Raman spectra showed that only Hematite (Fe_2O_3) and Magnetite (Fe_3O_4) were formed. According to Gaskell (1981), Wüstite (FeO) is thermodynamically unstable below 570°C. The equilibrium was determined using the assumption that only Hematite and Magnetite were formed. The reaction is written as

$$4Fe_3O_4 + O_2 \rightleftharpoons 6Fe_2O_3 \tag{4.1}$$

The data in Table 4.3 were used to find the equilibrium constant, k_p, from the following equations;

$$\ln k_p = -\frac{\Delta G_{298}}{RT_0} + \frac{\Delta H_0}{R}\left(\frac{1}{T_0} - \frac{1}{T}\right) + \frac{a_i}{R}\ln\frac{T}{T_0} + \frac{b_i}{2R}(T - T_0) + \frac{c_i}{6R}\left(T^2 - T_0^2\right) + \frac{d_i}{2R}\left(\frac{1}{T^2} - \frac{1}{T_0^2}\right) \tag{4.2}$$

and

$$\Delta H_0 = \Delta H_{298} - a_i T_0 - \frac{b_i T_0^2}{2} - \frac{c_i T_0^3}{3} + \frac{d_i}{T_0^2} \tag{4.3}$$

where T_0 = standard temperature = 298 K

T = temperature (K)

ΔG_{298} = standard free energy (cal/mol)

ΔH_{298} = standard enthalpy (cal/mol)

R = ideal gas constant = 1.9858775 ($cal/mol \cdot K$)

a_i, b_i, c_i *and* d_i = regression coefficients for chemical compound

Table 4.3 Data for reaction $4Fe_3O_4 + O_2 \rightleftharpoons 6Fe_2O_3$

Compound	ΔG_{298} (kcal/mol)	ΔH_{298} (kcal/mol)	$C_p = a + bT + \frac{d}{T^2}$ (cal/mol.K)
Fe_2O_3	-179.1	-198.5	$24.72 + 0.01604T - \frac{423400}{T^2}$
Fe_3O_4	-242.3	-266.9	$41.17 + 0.018824T - \frac{997500}{T^2}$
O_2	0	0	$8.27 + 0.000258T - \frac{187700}{T^2}$

The change in free energy, ΔG, can be expressed as

$$\Delta G_{298,rxn} = \Delta G_{298,prod} - \Delta G_{298,react} \tag{4.4}$$

Based on the reaction 4.1, Eq. 4.4 becomes

$$\Delta G_{298,rxn} = 6\left(\Delta G_{298,Fe_2O_3}\right) - 4\left(\Delta G_{298,Fe_3O_4}\right) - \Delta G_{298,O_2} \tag{4.5}$$

Therefore

$$\Delta G_{298,rxn} = 6(-179100) - 4(-242300) - 0$$

$$\Delta G_{298,rxn} = -105400\, cal/mol$$

Find the change in enthalpy, $\Delta H_{298,rxn}$

$$\Delta H_{298,rxn} = \Delta H_{298,prod} - \Delta H_{298,react} \tag{4.6}$$

$$\Delta H_{298,rxn} = 6\left(\Delta H_{298,Fe_2O_3}\right) - 4\left(\Delta H_{298,Fe_3O_4}\right) - \Delta H_{298,O_2} \tag{4.7}$$

$$\Delta H_{298,rxn} = 6(-198500) - 4(-266900) - 0$$

$$\Delta H_{298,rxn} = -123400\, cal/mol$$

Find the parameters for ΔC_p

$$C_{p_i} = a_i + b_i T + \frac{d_i}{T^2} \tag{4.8}$$

From

$$\Delta C_p = 6C_{p,Fe_2O_3} - 4C_{p,Fe_3O_4} - C_{p,O_2} \qquad (4.9)$$

Therefore,

a = -24.83 *cal/mol·K*

b = +0.020702 *cal/mol·K*^{2}

c = 0

d = +1.6373×10^6 *cal·K /mol*

From $k_p = \frac{1}{P_{O_2}}$, P_{O_2} was calculated and is shown in Table 4.4.

Table 4.4 Equilibrium constants and partial pressures of oxygen at equilibrium for various temperatures

T (K)	T (°C)	$\ln k_p$	k_p	$\frac{1}{k_p} = P_{O_2}$ (atm)
298	25	178.1032693	2.23495×10^{77}	4.47438×10^{-78}
363	90	139.0895845	2.54589×10^{60}	3.9279×10^{-61}
400	127	122.5164616	1.61519×10^{53}	6.19123×10^{-54}
500	227	89.88693975	1.08994×10^{39}	9.17483×10^{-40}
600	327	68.0025784	3.41306×10^{29}	2.92992×10^{-30}
673	400	56.07054268	2.24454×10^{24}	4.45526×10^{-25}
700	427	52.27681013	5.05278×10^{22}	1.97911×10^{-23}
800	527	40.41942515	3.58041×10^{17}	2.79297×10^{-18}
900	627	31.15690794	3.39839×10^{13}	2.94257×10^{-14}
1000	727	23.72337857	2.00878×10^{10}	4.97815×10^{-11}
2000	1727	-9.47330575	7.68769×10^{-5}	13007.81689

From Table 4.4, at 400°C the reaction thermodynamically predicts Hematite even if at very low oxygen pressure (4.45526×10^{-25} atm). However, it was found that Magnetite formed on the carbon steel surfaces which were exposed to

the environment which changes in oxygen concentration during the exposure. Therefore, kinetics must be significant with respect to the form of oxide produced.

4.1.3 Stainless Steel (SS 316)

The SEM images (Figure 4.9) of stainless steel show the oxide particles distributed on the surface after the 400°C exposure. The major area of the surface (dark area) was further analyzed by EDS as show in Figure 4.10, the oxygen characteristic peak is slightly higher than the peak of the baseline stainless steel which means that oxygen was adsorbed on the surface. The oxide particles (white spots) were also analyzed by EDS which shows the peaks of Fe, Cr and O, therefore the oxide particles might be iron oxide and chromium oxide. The appearances of both A-side and B-side are similar. Also there is not much difference in the EDS spectra.

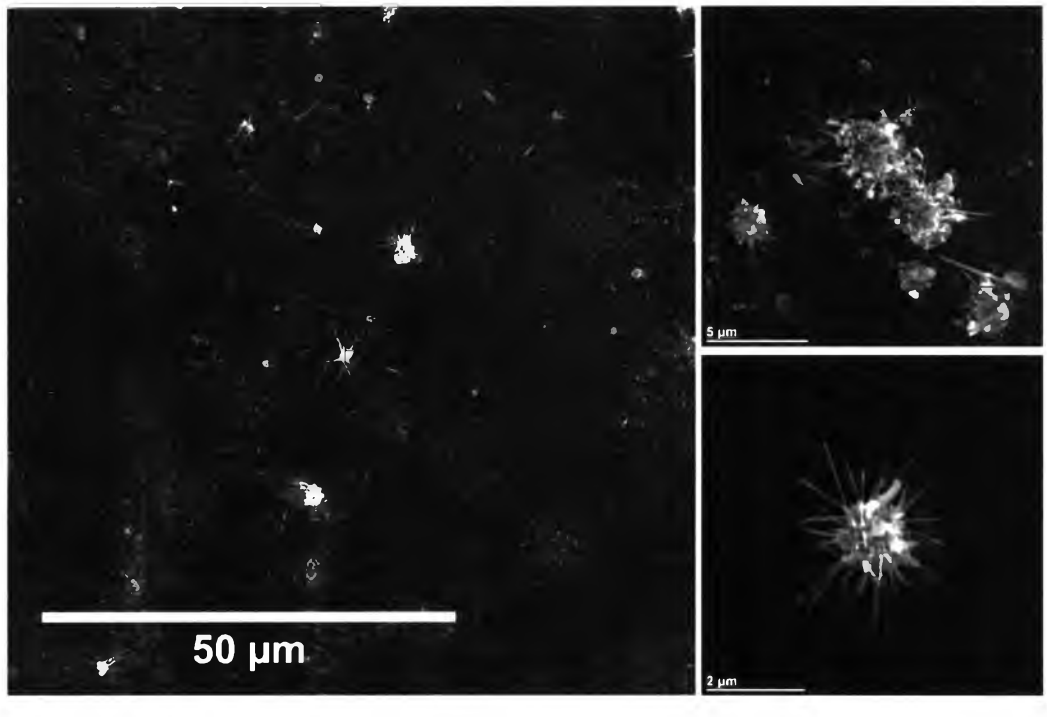

Figure 4.9 SEM images of stainless steel surface exposed to 400°C for 14 days.

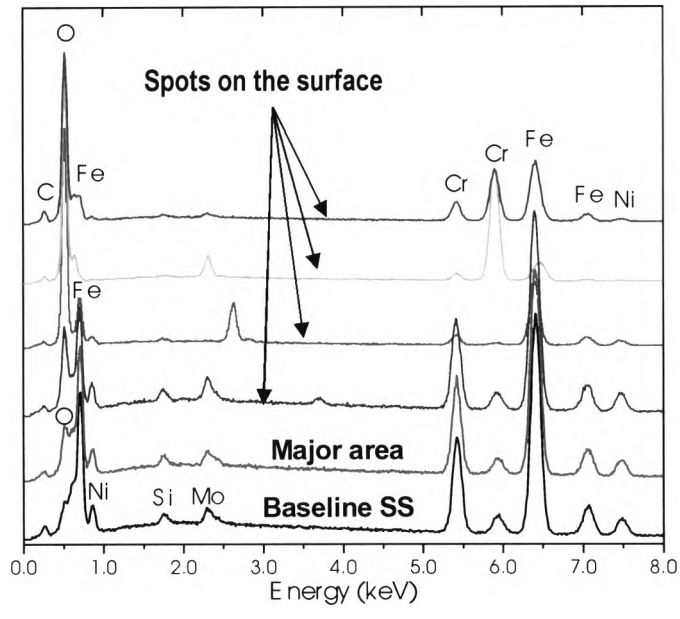

Figure 4.10 EDS spectra of stainless steel surface after the 400°C exposure.

4.1.4 Nickel Alloy (Alloy 625)

For nickel-alloy, SEM images and EDS spectra of both A-side and B-side are similar as illustrated in Figures 4.11 and 4.12, respectively. The EDS spectrum of the major area (dark area in SEM image) of the nickel-alloy surface, which was exposed to 400°C environment, shows slightly higher O peak intensity when compared to the baseline nickel-alloy indicating the adsorption of oxygen on the surface. The EDS spectra of the particles (white spots on the surface) show characteristic peaks of Ti which did not appear in the baseline spectrum. This might be because oxygen first adsorbed on the nickel alloy surface diffuses into the metal and forms oxide with titanium which was located below the surface. The oxide formed under the surface causes an expansion and then breaks through the surface.

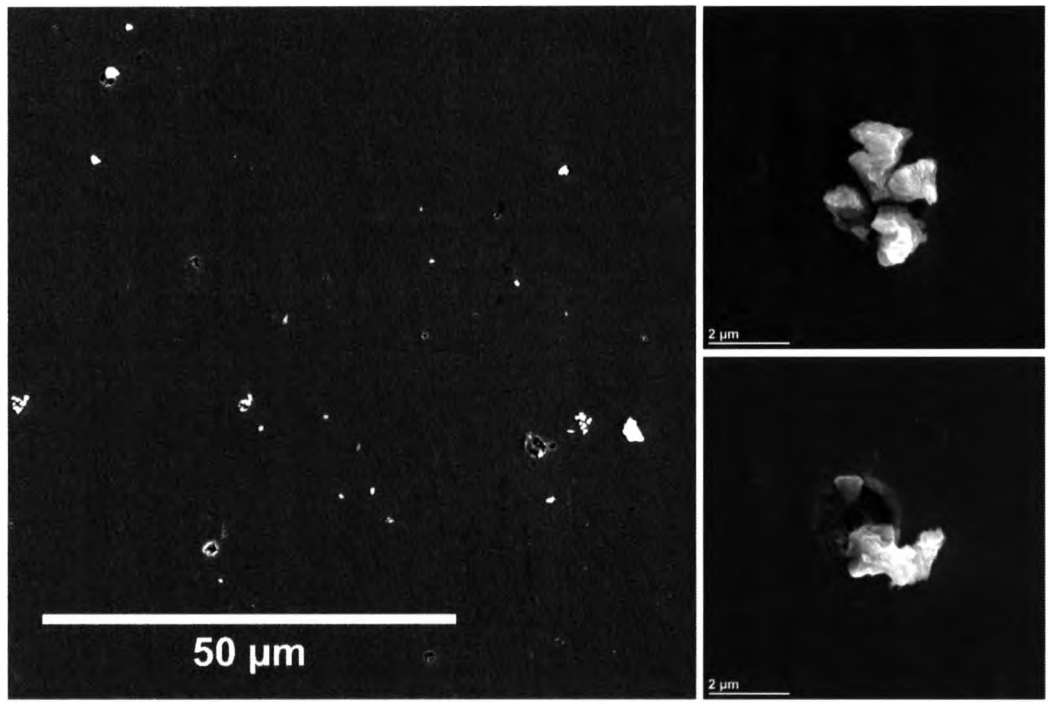

Figure 4.11 SEM images of nickel-alloy surfaces exposed to 400°C for 14 days.

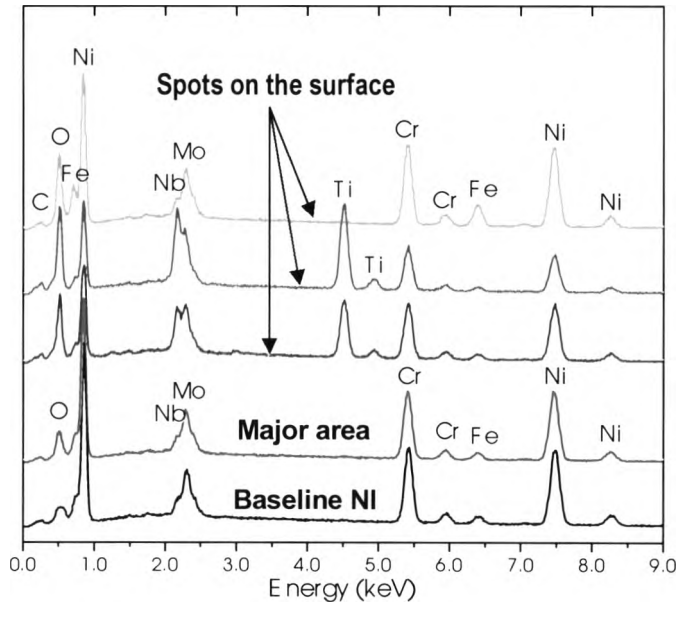

Figure 4.12 EDS spectra of nickel-alloy surface after the 400°C exposure.

4.2 Weight Gain on Samples and Thickness of Oxide Layers

Fresh polished samples including a membrane and a wire (extra required surface) were weighed before and after the exposure. The weight gain was then calculated. As the membrane oxidized on both sides (A-side and B-side), the weight gain per unit area was calculated based on the weight gain per unit area of the wire in the cavity (A-side) using the assumption that the weight gain per area on the wire is equal to the weight gain per area on the membrane inside the cavity (A-side). The weight gain on B-side was then calculated from the total weight gain on the membrane subtracted by the weight gain on the A-side. There was no significant weight gain on stainless steel and nickel-alloy at 400°C, as well as on carbon steel and stainless steel at 90°C exposure. The weight gain per unit area of each membrane is shown in Figure 4.13.

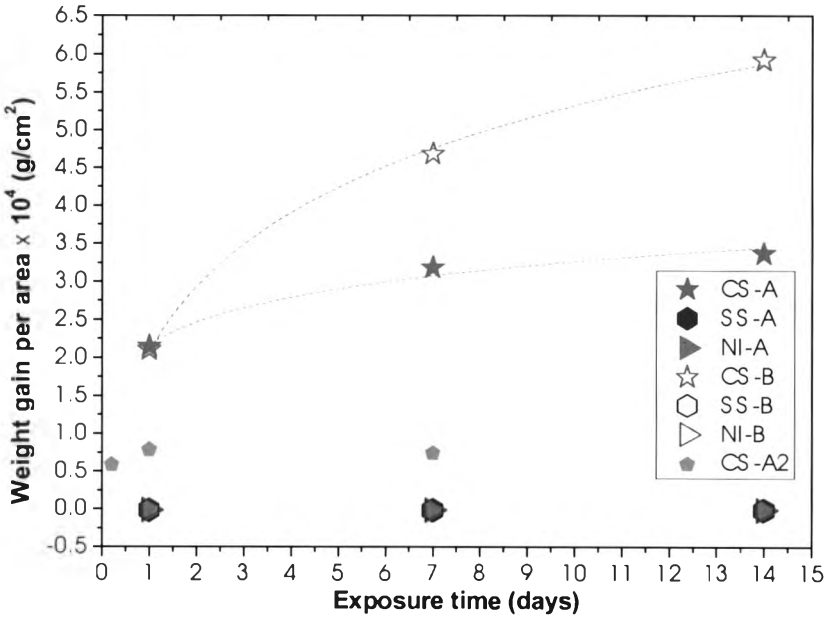

Figure 4.13 Relations between the weight gain per unit area and exposure time for the 400°C exposure samples.

The weight gain per unit area of each sample was used to calculate the thickness of oxide layer based on the assumption that the net weight gain of the sam-

ple is equal to the weight of oxygen uptake, the number of moles of oxygen can be found. The type of oxide on each surface used in the calculation was attained from the Raman spectroscopy result. Molecular weight and density of each type of oxides were applied in order to obtain the thickness of oxide layer. The result are provided in Figure 4.14.

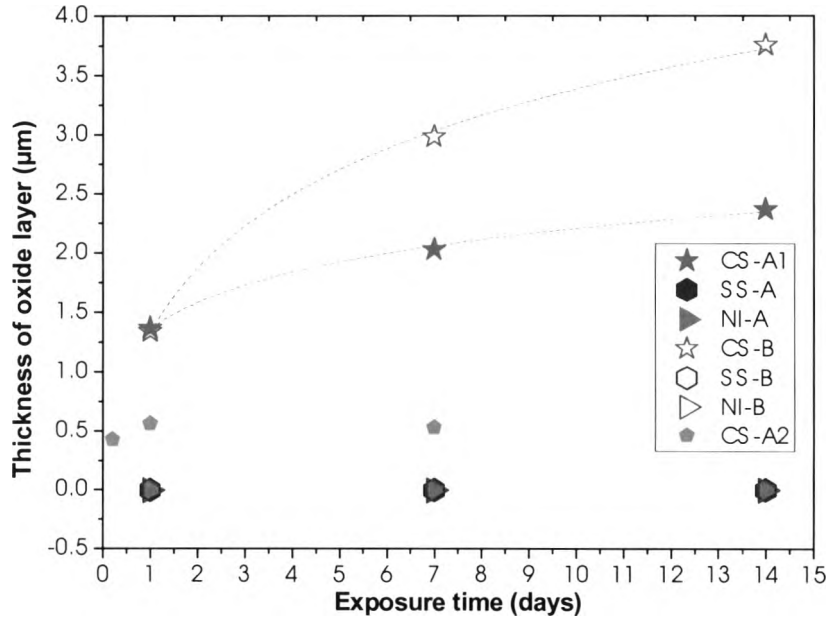

Figure 4.14 Relations between the thickness of oxide layer and exposure time for the 400°C exposure samples.

The three carbon steel membranes were cut and mounted in epoxy resin for cross-sectional analysis. The mounted membranes were sent to SEM analysis to measure the thickness of the oxide formed on each surface. The images (Figures 4.15-4.20) show the thicknesses of oxide on the surfaces, which were in agreement with the thicknesses from the calculation based on the weight gain per area. However, the thickness from each method is not completely the same, which might be because of non-uniformly formed oxide on the surface. Table 4.5 shows the thickness of oxide layer from the calculation compared to the average thickness from cross-sectioning analysis.

Table 4.5 Comparison between the thickness of oxide layer on carbon steel membrane (CS A106B) from calculation and from average cross-sectional analysis

Exposure time	Thickness of oxide layer (μm)			
	A-side		B-side	
	Calculated	Cross-sectioning	Calculated	Cross-sectioning
1 day	1.37	0.95	1.34	1.57
7 days	2.03	2.45	2.98	3.23
14 days	2.36	3.85-5.16*	3.75	4.43

*non-uniform thickness of oxide layer was found.

From Figure 4.19, the images show the oxide layer of the B-side which exposed for 14 days. There are two oxide layers on this surface; however, more analysis is required to identify the characteristics of individual layers.

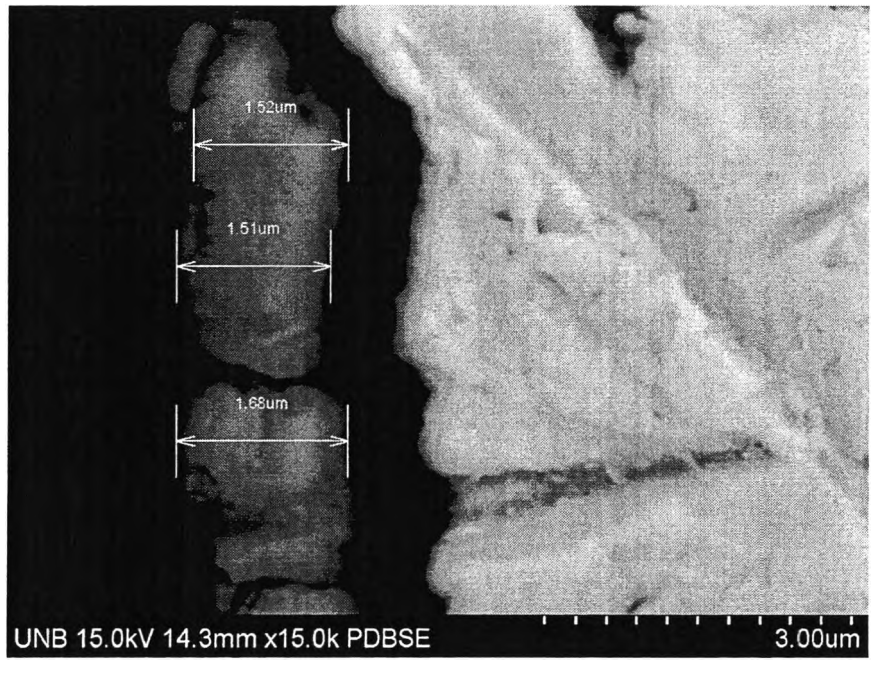

Figure 4.15 Cross-sectional image of the carbon steel membrane (B-side) exposed to 400°C for 1 day.

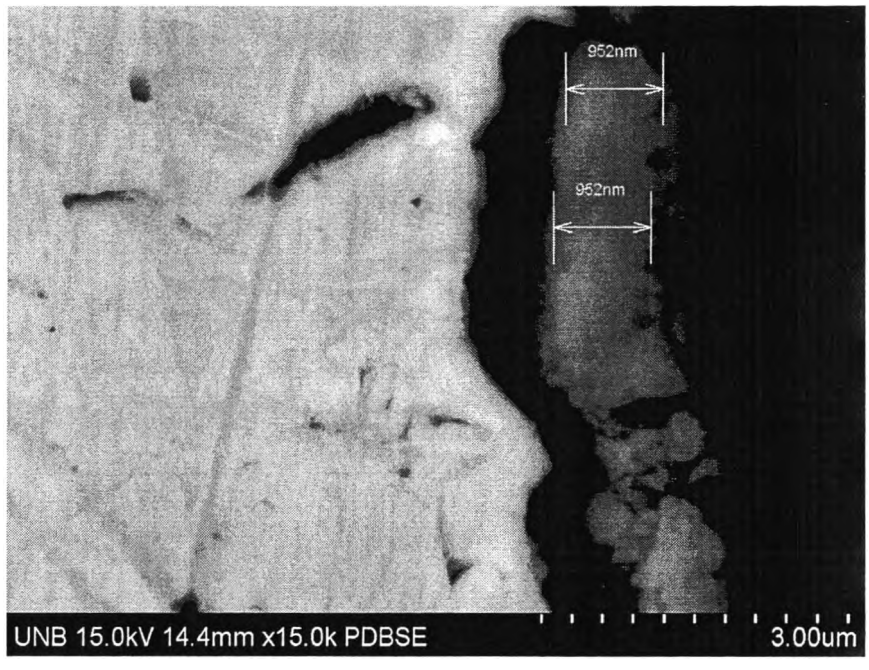

Figure 4.16 Cross-sectional image of the carbon steel membrane (A-side) exposed to 400°C for 1 day.

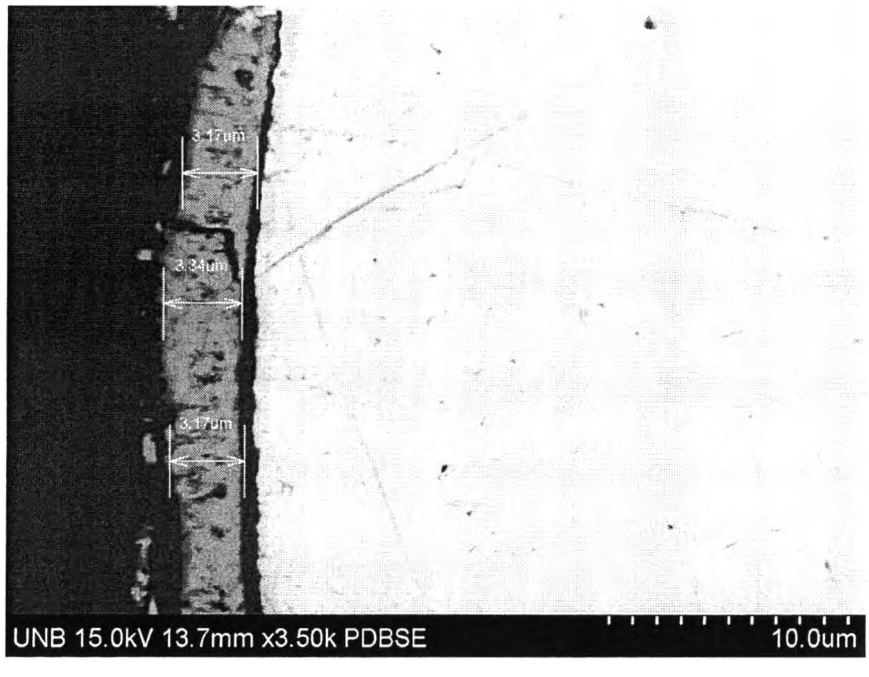

Figure 4.17 Cross-sectional image of the carbon steel membrane (B-side) exposed to 400°C for 7 days.

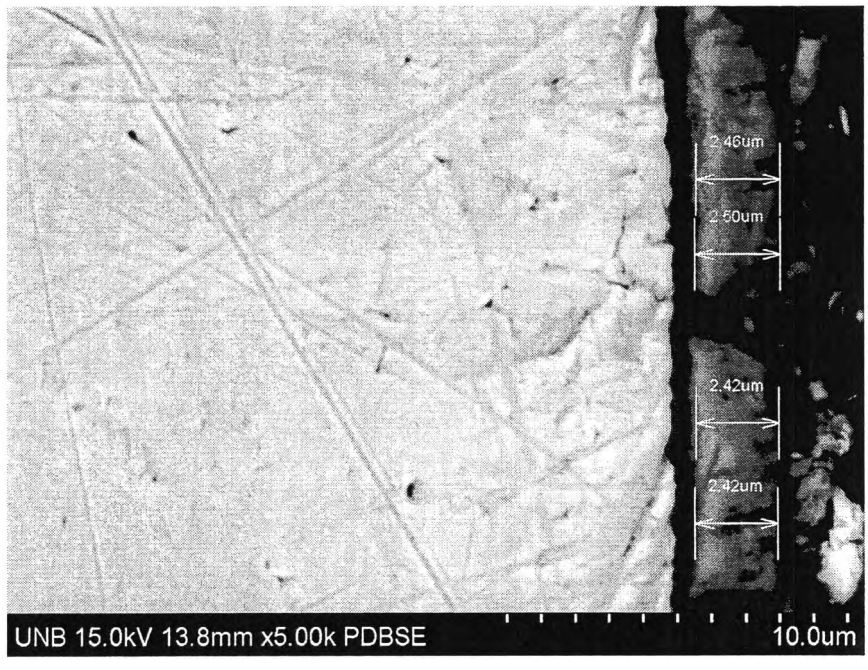

Figure 4.18 Cross-sectional image of the carbon steel membrane (A-side) exposed to 400°C for 7 days.

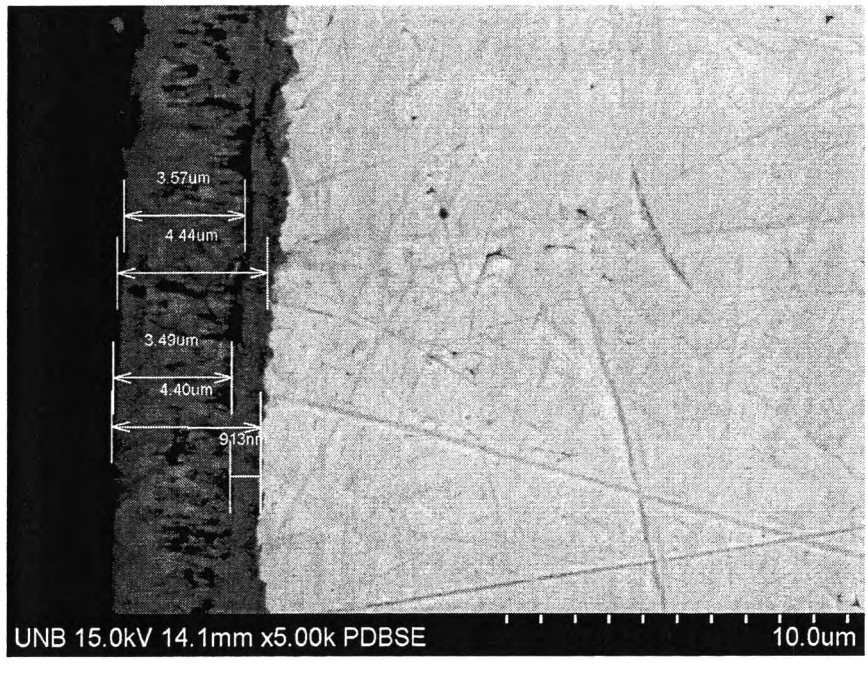

Figure 4.19 Cross-sectional image of the carbon steel membrane (B-side) exposed to 400°C for 14 days.

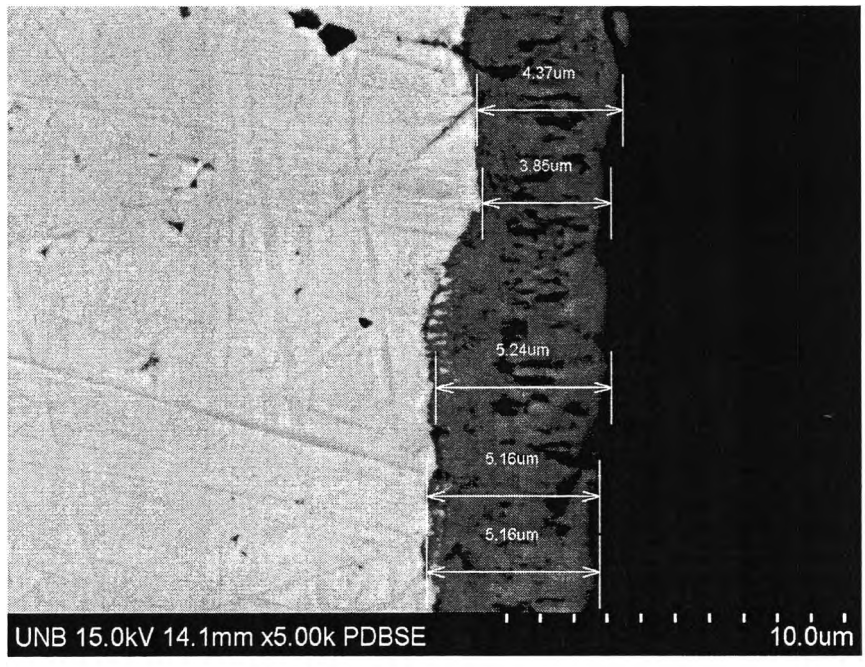

Figure 4.20 Cross-sectional image of the carbon steel membrane (A-side) exposed to 400°C for 14 days.

4.3 Kinetics of Oxide Formation

Below 570°C, the possible products of oxidation of carbon steel are Hematite and Magnetite. The schematic of iron oxide formation is shown in Figure 4.21. The reactions if iron to form Magnetite (Fe_3O_4) and Hematite (Fe_2O_3) are as follows:

$$3Fe + 2O_2 \rightarrow Fe_3O_4 \qquad (4.10)$$

$$2Fe + \frac{3}{2}O_2 \rightarrow Fe_2O_3 \qquad (4.11)$$

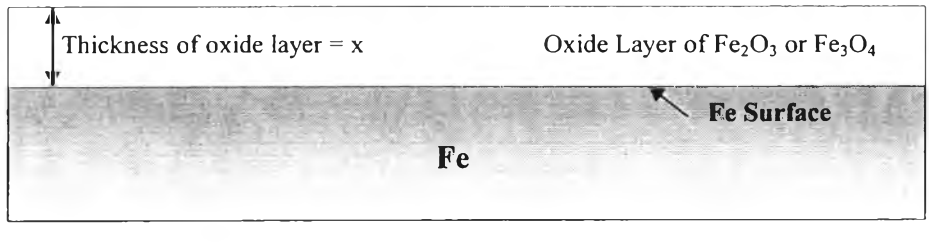

Figure 4.21 Schematic of iron oxide formed on iron surface.

4.3.1 Diffusion of Oxygen Through an Oxide Layer Control

Form the diffusivity equation;

$$-D_{O_2}\frac{dC_{O_2}}{dx} = -\frac{dN_{O_2}}{dt} \tag{4.12}$$

where D_{O_2} = the diffusivity of oxygen through an oxide layer

C_{O_2} = the concentration of oxygen in surroundings

N_{O_2} = moles of oxygen

x = the oxide layer thickness

t = time.

4.3.1.1 If Magnetite was Formed

From reaction 4.10,

$$-\frac{dN_{O_2}}{dt} = r_{Fe}\left(\frac{2}{3}\right) \tag{4.13}$$

where r_{Fe} = mole of Fe/unit time per area reacted.

And from $\frac{dm_{Fe}}{dt} = r_{Fe}MW_{Fe}$ (Mass Fe reacted/ unit time per area) r_{Fe} becomes

$$r_{Fe} = \frac{1}{MW_{Fe}}\frac{dm_{Fe}}{dt} \tag{4.14}$$

Substituting Eqs. 4.13 and 4.14 into Eq. 4.12 yields

$$-D_{O_2}\frac{dC_{O_2}}{dx} = \frac{2}{3MW_{Fe}}\frac{dm_{Fe}}{dt} \tag{4.15}$$

Rearrange Eq. 4-15 to get

$$-\frac{dC_{O_2}}{dx} = \frac{2}{3MW_{Fe}D_{O_2}}\frac{dm_{Fe}}{dt} \tag{4.16}$$

Integrating Eq. 4.16 yields

$$-C_{O_2} = \frac{2x}{3MW_{Fe}D_{O_2}}\frac{dm_{Fe}}{dt} \tag{4.17}$$

Rearranging Eq. 4.17 becomes

$$\frac{dm_{Fe}}{dt} = -\frac{3C_{O_2} MW_{Fe} D_{O_2}}{2x} \tag{4.18}$$

From Eq. 4.10, the rate of Fe_3O_4 formed is equal to one third of the rate of Fe reacted, therefore,

$$-\frac{1}{3}\frac{m_{Fe}}{MW_{Fe}} = \frac{m_{Fe_3O_4}}{MW_{Fe_3O_4}} \tag{4.19}$$

where m_{Fe} = the mass of Fe reacted

$m_{Fe_3O_4}$ = the mass of Fe_3O_4 formed

MW_{Fe} = the molecular weight of Fe

$MW_{Fe_3O_4}$ = the molecular weight of Fe_3O_4

Rearranging and dividing Eq. 4.19 by density of Fe_3O_4, $\rho_{Fe_3O_4}$ yields

$$V_{Fe_3O_4} = -\frac{1}{3}\frac{m_{Fe} MW_{Fe_3O_4}}{MW_{Fe}\rho_{Fe_3O_4}} \tag{4.20}$$

The change in oxide layer thickness by time is expressed as

$$\frac{dx}{dt} = -\frac{dm_{Fe}}{dt} \cdot V_{Fe_3O_4} \tag{4.21}$$

Substitution of Eqs. 4.18 and 4.20 into Eq. 4.21 yields

$$\frac{dx}{dt} = \left(-\frac{3C_{O_2} MW_{Fe} D_{O_2}}{2x}\right)\left(-\frac{1}{3}\frac{MW_{Fe_3O_4}}{MW_{Fe}\rho_{Fe_3O_4}}\right) \tag{4.22}$$

Thus,

$$\frac{dx}{dt} = \frac{1}{2}\frac{C_{O_2} D_{O_2} MW_{Fe_3O_4}}{x\rho_{Fe_3O_4}} \tag{4.23}$$

Integration of Eq. 4.23 yields

$$\frac{x^2}{2} = \frac{1}{2}\frac{C_{O_2} D_{O_2} MW_{Fe_3O_4} t}{\rho_{Fe_3O_4}} \tag{4.24}$$

or

$$x^2 = \frac{C_{O_2} D_{O_2} MW_{Fe_3O_4} t}{\rho_{Fe_3O_4}} \tag{4.25}$$

4.3.1.2 If Hematite was Formed

Reaction 4.11 can be written as

$$Fe + \frac{3}{4}O_2 \rightarrow \frac{1}{2}Fe_2O_3 \tag{4.26}$$

And the reaction rate is expressed as

$$-\frac{dN_{O_2}}{dt} = r_{Fe}\left(\frac{3}{4}\right) \tag{4.27}$$

Substituting Eqs. 4.27 and 4.14 into Eq. 4.12 yields

$$-D_{O_2}\frac{dC_{O_2}}{dx} = \frac{3}{4MW_{Fe}}\frac{dm_{Fe}}{dt} \tag{4.28}$$

Rearrange Eq. 4.28 to get

$$-\frac{dC_{O_2}}{dx} = \frac{3}{4MW_{Fe}D_{O_2}}\frac{dm_{Fe}}{dt} \tag{4.29}$$

Integrating Eq. 4.29 yields

$$-C_{O_2} = \frac{3x}{4MW_{Fe}D_{O_2}}\frac{dm_{Fe}}{dt} \tag{4.30}$$

Rearrangement of Eq. 4.30 yields

$$\frac{dm_{Fe}}{dt} = -\frac{4C_{O_2}MW_{Fe}D_{O_2}}{3x} \tag{4.31}$$

From reaction 4.26, the rate of Fe_2O_3 formed is equal to a half of the rate of Fe reacted, therefore,

$$-\frac{1}{2}\frac{m_{Fe}}{MW_{Fe}} = \frac{m_{Fe_2O_3}}{MW_{Fe_2O_3}} \tag{4.32}$$

where m_{Fe} = the mass of Fe reacted

$m_{Fe_2O_3}$ = the mass of Fe_2O_3 formed

MW_{Fe} = the molecular weight of Fe

$MW_{Fe_2O_3}$ = the molecular weight of Fe_2O_3

Rearranging and dividing Eq. 4.32 by density of Fe_2O_3, $\rho_{Fe_2O_3}$ yields

$$V_{Fe_2O_3} = -\frac{1}{2}\frac{m_{Fe}MW_{Fe_2O_3}}{MW_{Fe}\rho_{Fe_2O_3}} \tag{4.33}$$

The change in oxide layer thickness by time is expressed as

$$\frac{dx}{dt} = -\frac{dm_{Fe}}{dt} \cdot V_{Fe_2O_3} \tag{4.34}$$

Substitution of Eqs. 4.31 and 4.33 into Eq 4.34 yields

$$\frac{dx}{dt} = \left(-\frac{4C_{O_2} MW_{Fe} D_{O_2}}{3x} \right) \left(-\frac{1}{2} \frac{MW_{Fe_2O_3}}{MW_{Fe} \rho_{Fe_2O_3}} \right) \tag{4.35}$$

Thus,

$$\frac{dx}{dt} = \frac{4}{6} \frac{C_{O_2} D_{O_2} MW_{Fe_2O_3}}{x \rho_{Fe_2O_3}} \tag{4.36}$$

Integration of Eq. 4.36 yields

$$\frac{x^2}{2} = \frac{4}{6} \frac{C_{O_2} D_{O_2} MW_{Fe_2O_3} t}{\rho_{Fe_2O_3}} \tag{4.37}$$

or

$$x^2 = \frac{4}{3} \frac{C_{O_2} D_{O_2} MW_{Fe_2O_3} t}{\rho_{Fe_2O_3}} \tag{4.38}$$

4.3.2 Chemical Reaction Control

4.3.2.1 If Magnetite was Formed

From reaction 4.10, rate of reaction is

$$-\frac{dN_{O_2}}{dt} = r_{Fe} \left(\frac{2}{3} \right) \tag{4.39}$$

Assume $r_{Fe} = rC_{O_2}$, therefore, the change in mass of Fe is

$$\frac{dm_{Fe}}{dt} = r_{Fe} m_{Fe} = rC_{O_2} m_{Fe} \tag{4.40}$$

The change in oxide layer thickness by time is written as

$$\frac{dx}{dt} = \frac{1}{3} \frac{dm_{Fe}}{dt} \frac{MW_{Fe_3O_4}}{MW_{Fe} \rho_{Fe_3O_4}} \tag{4.41}$$

Substituting Eq. 4.40 into Eq. 4.41

$$\frac{dx}{dt} = \frac{1}{3} \frac{rC_{O_2} m_{Fe} MW_{Fe_3O_4}}{MW_{Fe} \rho_{Fe_3O_4}} \tag{4.42}$$

Integration of Eq. 4.42 yields

$$x = \frac{1}{3}\frac{rC_{O_2} m_{Fe} MW_{Fe_3O_4}}{MW_{Fe}\rho_{Fe_3O_4}} t \tag{4.43}$$

4.3.2.1 If Hematite was Formed

From reaction 4.10, rate of reaction is

$$-\frac{dN_{O_2}}{dt} = r_{Fe}\left(\frac{3}{4}\right) \tag{4.44}$$

The change in oxide layer thickness by time is written as

$$\frac{dx}{dt} = \frac{4}{6}\frac{dm_{Fe}}{dt}\frac{MW_{Fe_2O_3}}{MW_{Fe}\rho_{Fe_2O_3}} \tag{4.45}$$

Substituting Eq. 4.40 into equation 4.45

$$\frac{dx}{dt} = \frac{4}{6}\frac{rC_{O_2} m_{Fe} MW_{Fe_2O_3}}{MW_{Fe}\rho_{Fe_2O_3}} \tag{4.46}$$

Integration of Eq. 4.46 yields

$$x = \frac{4}{6}\frac{rC_{O_2} m_{Fe} MW_{Fe_2O_3}}{MW_{Fe}\rho_{Fe_2O_3}} t \tag{4.47}$$

4.3.3 Kinetics of Oxide Formation on Carbon Steels Exposed to an Atmosphere with No Change in O_2 Concentration (B-side)

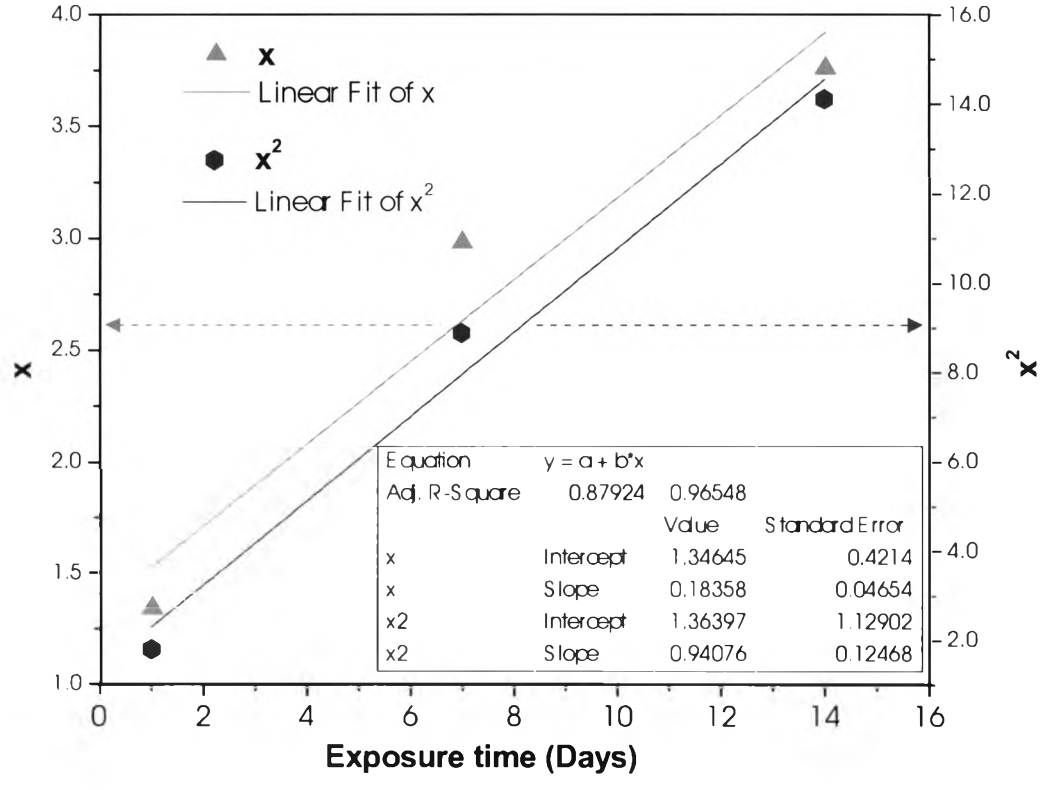

Figure 4.22 Relation between x or x^2 and exposure time for B-side of the 400°C exposure samples.

From the relation between the oxide thickness and time (Figure 4.22), it shows that the rate of oxide formation on carbon steel A106B at 400°C in an atmosphere with no change in O_2 concentration (B side) can be explained by diffusion of oxygen through the oxide layer. From the previous surface information, the oxide formed on this B side is Hematite (Fe_2O_3).

From Linear fit of x^2 and based on Hematite formed, D_{O_2} was determined;

Slope of the Linear fit = 0.94076 μm^2/day = 1.089×10^{-17} m^2/s.

From Eq. 4.38, $x^2 = \frac{4}{3}\frac{C_{O_2} D_{O_2} MW_{Fe_2O_3}}{\rho_{Fe_2O_3}} t$, and the parabolic rate; $x^2 = k_p t + c$, Therefore

$$slope = k_p = \frac{4}{3}\frac{C_{O_2} D_{O_2} MW_{Fe_2O_3}}{\rho_{Fe_2O_3}} \qquad (4.48)$$

where; x is the thickness of the oxide layer,

t is exposure time,

k_p is the parabolic rate constant,

$MW_{Fe_2O_3}$ is the molecular weight of Fe_2O_3 = 159.69 g/mol,

$\rho_{Fe_2O_3}$ is the density of Fe_2O_3 = 5.242 g/cm^3 = 5.242× 10^6 g/m^3,

C_{O_2} is the concentration of oxygen:

$C_{O_2\ at\ 25°C}$ = 8.59 moles/m^3, $C_{O_2\ at\ 400°C}$ = 3.80 mol/m^3

D_{O_2} is the diffusivity of oxygen through the oxide layer (to be found)

Using the data from the plot of x^2 versus t and Eq. 4.48,

$$slope = k_p = \frac{4}{3}\frac{C_{O_2} D_{O_2} MW_{Fe_2O_3}}{\rho_{Fe_2O_3}} = 1.089\times10^{-17}$$

$$k_p = 1.089\times10^{-17}\, m^2/s$$

$$D_{O_2} = \left(1.089\times10^{-17}\right)\times\frac{3}{4}\left(\frac{5.242\times10^6}{(3.80)(159.69)}\right) m^2/s$$

$$D_{O_2} = 7.05545\times10^{-14}\, m^2/s$$

The diffusivity of oxygen through oxide layer in atmospheric air at 400°C is 7.05545×10^{-14}m^2/s and the parabolic rate, k_p, is $1.089\times10^{-17}\, m^2/s$.

This diffusivity was further used in the determination of kinetics of oxide formation in an atmosphere with change in O_2 concentration.

4.3.4 Kinetics of Oxide Formation on Carbon Steels Exposed to an Atmosphere with Change in O_2 Concentration (A-side)

In this section, the rate of oxide formed in each set of the experiments was determined. From the material characterization results, the assumption of all oxide is Hematite was applied to the experimental set 1 and the assumption of all oxide is Magnetite was applied to the experimental set 2.

The diffusivity of oxygen through the oxide layer from the last section ($D_{O_2} = 7.05545 \times 10^{-14} m^2/s$) was used to determined the kinetics in both parts of experiments. $C_{O_2\ at\ 25°C}$ = 8.59 moles/m^3 was used as an initial oxygen concentration ($C_{O_2,0}$) since the cavity was installed at room temperature and atmospheric pressure before the temperature was raised up to 400°C. The pressure inside the cavity was calculated using concentration of air inside the cavity and ideal gas law (PV=nRT).

4.3.4.1 Kinetics of Oxide Formation in Experimental Set 1 (A-side-1)

Assuming all oxides formed are Fe_2O_3.

$$\text{moles of } O_2 \text{ in boundary layer} = \frac{3}{2}\frac{\rho_{Fe_2O_3} Ax}{MW_{Fe_2O_3} V_C} \tag{4.49}$$

where x = oxide layer thickness = boundary layer thickness

A = total exposed area inside the cavity

V_C = volume of the cavity (m^3)

The concentration of oxygen inside the cavity based on oxygen reacted to form the boundary layer becomes

$$C_{O_2}(x) = C_{O_2,0} - \frac{3}{2}\frac{\rho_{Fe_2O_3} Ax}{MW_{Fe_2O_3} V_C} \tag{4.50}$$

Substituting Eq. 4.50 into Eq. 4.36 yields

$$\frac{dx}{dt} = \frac{4}{6}\frac{D_{O_2} MW_{Fe_2O_3}}{x\rho_{Fe_2O_3}} C_{O_2,0}\left(1 - \frac{3}{2}\frac{\rho_{Fe_2O_3} Ax}{MW_{Fe_2O_3} V_C C_{O_2,0}}\right) \tag{4.51}$$

Rearranging Eq. 4.51 obtains

$$\frac{x}{\left(1-\frac{3}{2}\frac{\rho_{Fe_2O_3}Ax}{MW_{Fe_2O_3}V_C C_{O_2,0}}\right)}dx=\frac{2}{3}\frac{D_{O_2}MW_{Fe_2O_3}C_{O_2,0}}{\rho_{Fe_2O_3}}dt \qquad (4.52)$$

Integration of Eq. 4.52 yields

$$\int_0^x \frac{x}{\left(1-\frac{3}{2}\frac{\rho_{Fe_2O_3}Ax}{MW_{Fe_2O_3}V_C C_{O_2,0}}\right)}dx=\int_0^t \frac{2}{3}\frac{D_{O_2}MW_{Fe_2O_3}C_{O_2,0}}{\rho_{Fe_2O_3}}dt \qquad (4.53)$$

From integration formula

$$\int \frac{x}{ax+b}dx=\frac{x}{a}-\frac{b}{a^2}\ln(ax+b)$$

Let

$$a=-\frac{3}{2}\frac{\rho_{Fe_2O_3}A}{MW_{Fe_2O_3}V_C C_{O_2,0}}$$

$$b=+1.0$$

$$c=\frac{2}{3}\frac{D_{O_2}MW_{Fe_2O_3}C_{O_2,0}}{\rho_{Fe_2O_3}}$$

Eq. 4.53 becomes

$$\frac{x}{a}-\frac{b}{a^2}\ln(ax+b)=ct \qquad (4.54)$$

Multiplying both sides by "a" yields

$$x-\frac{b}{a}\ln(ax+b)=act \qquad (4.55)$$

Take the following values to evaluate the parameters in Eq. 4.55;

$V_C = 1.3\times10^{-5}\ m^3$ $\qquad$ $D_{O_2} = 7.05545\times10^{-14}\ m^2/s$

$A = 26.417\times10^{-4}\ m^2$ $\qquad$ $MW_{Fe_2O_3} = 159.69\ g/mol$

$C_{O_2,0} = 8.59\ mol/m^3$ $\qquad$ $\rho_{Fe_2O_3} = 5.242\times10^{6}\ g/m^3$

Therefore, $a = 2.12\times10^{6}\ m^{-1}$, $b = +1.0$, and $c = 6.75\times10^{-18}\ m^2/s$.

The plot of oxide layer thickness (x) versus exposure time (t) from Eq. 4.55 is shown in Figure 4.23. It shows that the actual oxide thickness formed on carbon steel is much higher than the thickness attained from Eq. 4.55, this

might be because the oxygen concentration inside the cavity which used in the calculation ($C_{O_2}(x)$) is different from the actual O_2 concentration. Also the amount oxygen in the cavity was not enough to form all the oxide. The possible reasons for these are; 1) some changes in oxygen concentration occurred within the cavity at the initial step and during the exposure (i.e. leaking), 2) some oxides formed could be Fe_3O_4 (different from the assumption that all oxides formed are Fe_2O_3), 3) the diffusivity of oxygen through the Fe_2O_3 layer on the B-side was uses in the calculation and it may not be the same as the diffusivity of oxygen on the A-side because of the difference of oxygen concentration (different driving force), and 4) the oxide layer thicknesses on membrane and wire may not be identical due to the differences in shape and elemental composition.

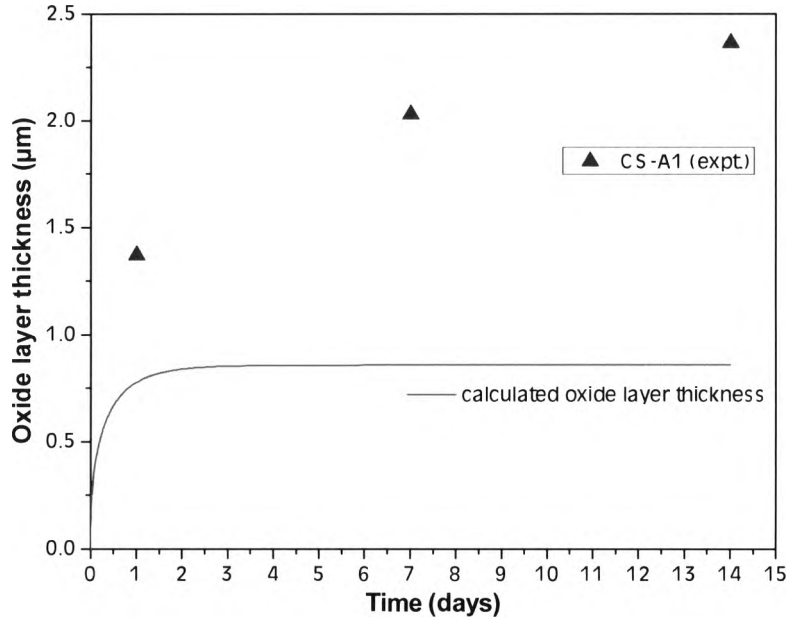

Figure 4.23 The plot of oxide layer thickness versus time of carbon steel (A-side-1).

The concentration of air and concentration of O_2 versus time is shown in Figure 4.24. The oxygen concentration, $C_{O_2}(x)$, was calculated form Eq. 4.50. The concentration of air was then calculated from the decreasing of O_2 concentration. The concentration of air was further used (with the ideal gas law) to calculate pressure inside the cavity showing in Figure 4.25.

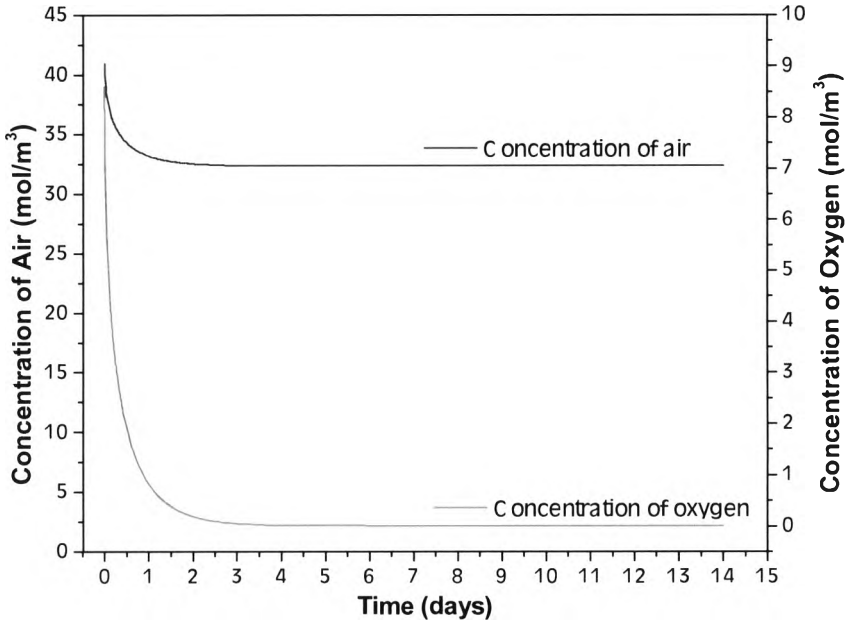

Figure 4.24 Relations between concentrations of air and oxygen inside the cavity and exposure time of the set 1 experiment.

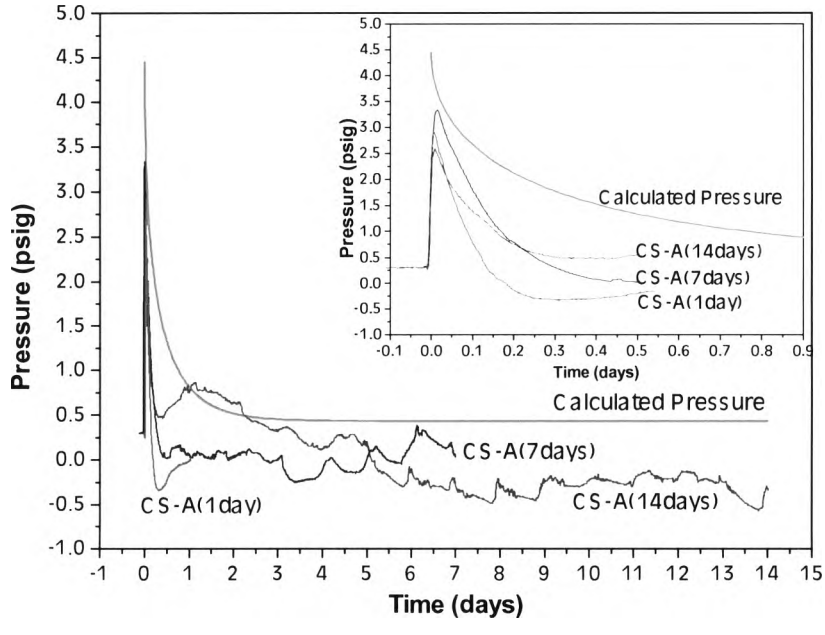

Figure 4.25 Relations between pressure inside the cavity and exposure time of the set 1 experiment.

Figure 4.25 shows the comparison of the actual pressures at various exposure periods and the calculated pressure. As can be seen, the initial decline of the actual pressure is faster than that of the calculated one. After the drop, the actual pressures stay around an atmospheric pressure. There are two possibilities for the decrease in pressure; firstly, because of the oxidation reaction, and secondly, of leaking. Since the measured oxide layer thickness was observed to be higher, O_2 might diffuse into the cavity during the exposure.

In addition, the initial actual pressures were found to be lower than the calculated pressure suggesting that there might be because of leaking. As the test section was heated up from room temperature to 400°C taken about 45 minutes, it is possible that some O_2 in the system was consumed to oxidize the steel before the temperature reached 400°C.

4.3.4.2 Kinetics of Oxide Formation in Experimental Set 2 (A-side-2)

Assuming all oxides formed are Fe_2O_3,

$$\text{moles of } O_2 \text{ in boundary layer} = 2\frac{\rho_{Fe_3O_4} Ax}{MW_{Fe_3O_4} V_C} \tag{4.56}$$

where x = oxide layer thickness = boundary layer thickness

A = total exposed area inside the cavity

V_C = volume of the cavity (m^3)

The concentration of oxygen inside the cavity based on oxygen reacted to form the boundary layer becomes

$$C_{O_2}(x) = C_{O_2,0} - 2\frac{\rho_{Fe_3O_4} Ax}{MW_{Fe_3O_4} V_C} \tag{4.57}$$

Substituting Eq. 4.57 into Eq. 4.23 yields

$$\frac{dx}{dt} = \frac{1}{2}\frac{D_{O_2} MW_{Fe_3O_4}}{x\rho_{Fe_3O_4}} C_{O_2,0} \left(1 - 2\frac{\rho_{Fe_3O_4} Ax}{MW_{Fe_3O_4} V_C C_{O_2,0}}\right) \tag{4.58}$$

Rearranging Eq.4.58 obtains

$$\frac{x}{\left(1 - 2\frac{\rho_{Fe_3O_4} Ax}{MW_{Fe_3O_4} V_C C_{O_2,0}}\right)} dx = \frac{1}{2}\frac{D_{O_2} MW_{Fe_3O_4} C_{O_2,0}}{\rho_{Fe_3O_4}} dt \tag{4.59}$$

Integration of Eq. 4.59 yields

$$\int_0^x \frac{x}{\left(1-2\dfrac{\rho_{Fe_3O_4}Ax}{MW_{Fe_3O_4}V_C C_{O_2,0}}\right)}dx = \int_0^t \frac{1}{2}\frac{D_{O_2}MW_{Fe_3O_4}C_{O_2,0}}{\rho_{Fe_3O_4}}dt \qquad (4.60)$$

By definition,

$$\int \frac{x}{ax+b}dx = \frac{x}{a} - \frac{b}{a^2}\ln(ax+b)$$

Let

$$a = -2\frac{\rho_{Fe_3O_4}A}{MW_{Fe_3O_4}V_C C_{O_2,0}}$$

$$b = +1.0$$

$$c = \frac{1}{2}\frac{D_{O_2}MW_{Fe_3O_4}C_{O_2,0}}{\rho_{Fe_3O_4}}$$

Eq. 4.60 becomes

$$\frac{x}{a} - \frac{b}{a^2}\ln(ax+b) = ct \qquad (4.61)$$

Multiply both sides by "*a*" yields

$$x - \frac{b}{a}\ln(ax+b) = act \qquad (4.62)$$

Take the following values to evaluate the parameters in Eq. 4.62;

$V_1 = 1.3\times10^{-5}\,m^3$ $\quad C_{O_2,0} = 8.59\,mol/m^3$

$A_1 = 2.64\times10^{-3}\,m^2$ $\quad D_{O_2} = 7.05545\times10^{-14}\,m^2/s$

$V_2 = 1.3\times10^{-5}\,m^3$ $\quad MW_{Fe_3O_4} = 231.553\,g/mol$

$A_2 = 2.59\times10^{-3}\,m^2$ $\quad \rho_{Fe_3O_4} = 5.17\times10^{6}\,g/m^3$

Therefore,

$a_1 = \ 1.06\times10^{6}\,m^{-1}$, $a_2 = \ 1.06\times10^{6}\,m^{-1}$

$b_1 = +1.0, b_2 = +1.0$

$c_1 = 1.36\times10^{17}\,m^2/s$, $c_2 = 1.36\times10^{17}\,m^2/s$

In the experimental set 2, the test section was changed therefore the volume of the cavity was changed. The Eq. 4.62 was plotted using the different V_C's. However, V_1/A_1 and V_2/A_2 are similar, so the plots almost overlap each other as shown in

Figure 4.26. As observed, the actual oxide thickness is lower than that obtained from Eq. 4.62 at a given exposure time. The concentrations of oxygen and air inside the cavity were calculated and plotted as shown in Figure 4.27.

Figure 4.28 shows the discrepancy in pressure inside the cavity between the actual and calculated pressures of the experimental set 2. When compared with those of the experimental set 1, the actual pressures were less declined. This might be due to the application of sealants. Therefore, if there were some leaks, it should be leaking out at the beginning (less than 2 days) of the exposure.

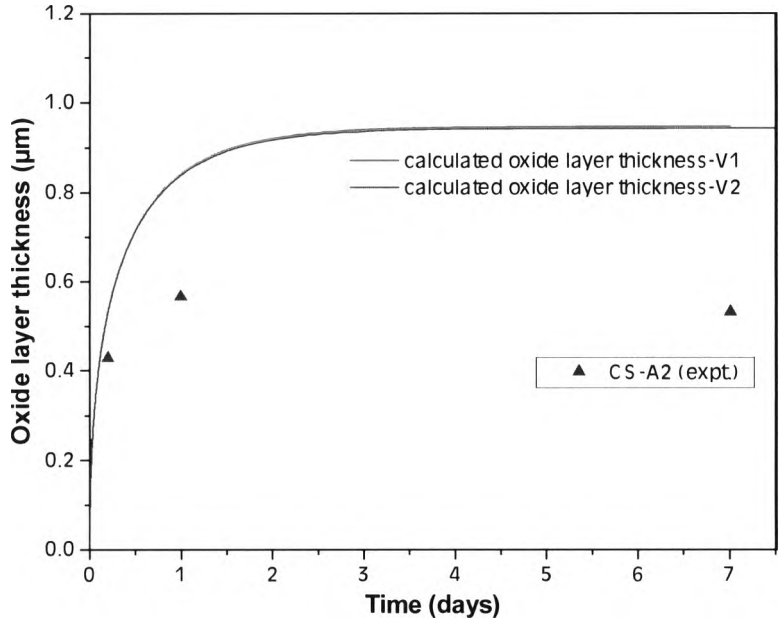

Figure 4.26 The plot of oxide layer thickness versus time of carbon steel (A-side-2).

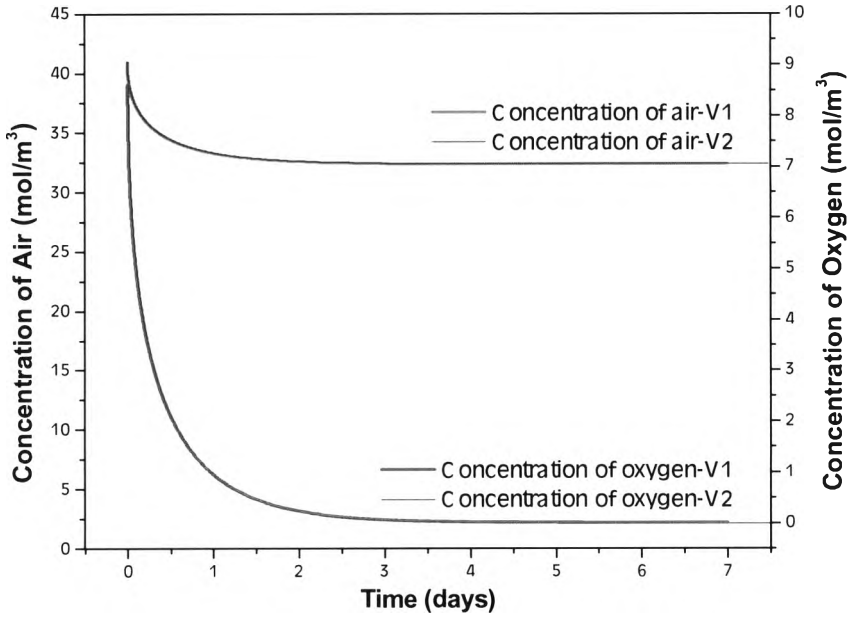

Figure 4.27 Relations between concentrations of air and oxygen inside the cavity and exposure time of the set 2 experiment.

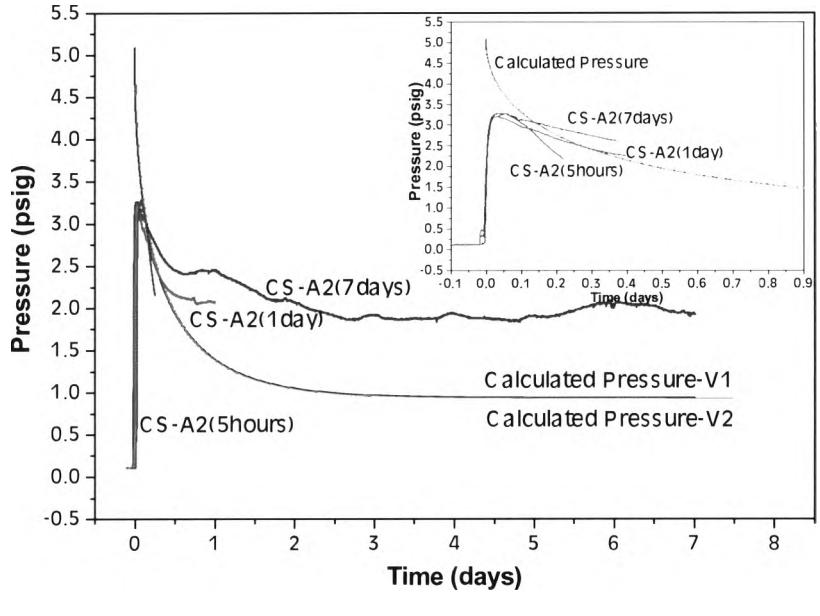

Figure 4.28 Relations between pressure inside the cavity and exposure time of the set 2 experiment.